

Geophysical Research Letters®

RESEARCH LETTER

10.1029/2021GL094183

Key Points:

- Global patterns and trends in magnitude, timing, and frequency of dry and humid-heat extremes in ERA5 compare well with HadISD station data
- Largest increases in frequency, intensity, and months of occurrence of dry- and humid-heat extremes in tropical and Arctic regions
- Stronger trends in population exposure to extreme humid-heat relative to dry-heat and greater amplification during recent El Niños

Supporting Information:

Supporting Information may be found in the online version of this article.

Correspondence to:

C. D. W. Rogers,
cassandra.rogers@wsu.edu

Citation:

Rogers, C. D. W., Ting, M., Li, C., Kornhuber, K., Coffel, E. D., Horton, R. M., et al. (2021). Recent increases in exposure to extreme humid-heat events disproportionately affect populated regions. *Geophysical Research Letters*, 48, e2021GL094183. <https://doi.org/10.1029/2021GL094183>

Received 10 MAY 2021
Accepted 16 SEP 2021

Recent Increases in Exposure to Extreme Humid-Heat Events Disproportionately Affect Populated Regions

Cassandra D. W. Rogers¹ , Mingfang Ting² , Cuihua Li², Kai Kornhuber^{2,3} , Ethan D. Coffel⁴, Radley M. Horton², Colin Raymond⁵ , and Deepti Singh¹ 

¹School of the Environment, Washington State University, Vancouver, WA, USA, ²Lamont-Doherty Earth Observatory, Columbia University, Palisades, NY, USA, ³Earth Institute, Columbia University, Palisades, NY, USA, ⁴Department of Geography and the Environment, Syracuse University, Syracuse, NY, USA, ⁵Jet Propulsion Laboratory/California Institute of Technology, Pasadena, CA, USA

Abstract Extreme heat research has largely focused on dry-heat, while humid-heat that poses a substantial threat to human-health remains relatively understudied. Using hourly high-resolution ERA5 reanalysis and HadISD station data, we provide the first spatially comprehensive, global-scale characterization of the magnitude, seasonal timing, and frequency of dry- and wet-bulb temperature extremes and their trends. While the peak dry- and humid-heat extreme occurrences often coincide, their timing differs in climatologically wet regions. Since 1979, dry- and humid-heat extremes have become more frequent over most land regions, with the greatest increases in the tropics and Arctic. Humid-heat extremes have increased disproportionately over populated regions (~5.0 days per-person per-decade) relative to global land-areas (~3.6 days per-unit-land-area per-decade) and population exposure to humid-heat has increased at a faster rate than to dry-heat. Our study highlights the need for a multivariate approach to understand and mitigate future harm from heat stress in a warming world.

Plain Language Summary Combined high temperature and humidity can be more dangerous to humans and wildlife relative to high temperature alone. There are known physiological limits to humid-heat and adverse impacts on human-health and performance can be felt well below those limits. Thus, it is important we understand their climatological characteristics and recent changes. Prior research on heat extremes has largely focused on dry-heat. Using two high-spatial resolution datasets, we provide a global-scale characterization of the magnitude, seasonal timing, and frequency of dry- and humid-heat extremes and their historical trends. While dry- and humid-heat extremes occur at the same time of the year in most regions, their timing differs by multiple months in tropical regions with high rainfall. Over the past four decades, dry- and humid-heat extremes have become more frequent over most land regions, with the greatest increases in the tropics and Arctic. Since 1979, each person, on average, has experienced an increase of approximately five additional extreme humid-heat days per-decade. These increases are concentrated over densely populated regions in the tropics and sub-tropics, where humid-heat levels are already high. Our results emphasize the increasing risk from dangerous heat stress, particularly in vulnerable regions of the world.

1. Introduction

Extreme heat can have devastating impacts on built and natural environments including crop losses, wild-fire risk, infrastructure damage, and wildlife mortality (e.g., Kornhuber et al., 2020; McEvoy et al., 2012; van der Velde et al., 2010; Webb et al., 2010), and can impact human-health (Hoegh-Guldberg et al., 2018; Xu et al., 2016). The world has become increasingly exposed to heat due to climate change (IPCC, 2013; Meehl & Tebaldi, 2004; Perkins-Kirkpatrick & Lewis, 2020). Recent research has largely characterized extreme heat using temperature alone (e.g., Perkins et al., 2012; Perkins-Kirkpatrick & Lewis, 2020; Russo et al., 2014). However, humidity exacerbates extreme heat impacts, particularly on human-health and labor-productivity. While literature on observed and projected humid-heat has emerged recently (e.g., Buzan & Huber, 2020; Raymond et al., 2020), a comprehensive assessment of their societally relevant characteristics and observed changes at high spatial and temporal resolution is lacking.

Humid-heat is the combined effect of temperature and humidity, commonly measured by wet-bulb temperature (Buzan et al., 2015). Humid-heat is particularly important when considering human-health and performance. Prolonged exposure above a wet-bulb temperature of 35°C is theoretically unsustainable (Hanna & Tait, 2015; Sherwood & Huber, 2010) and can result in heat-related mortality and illnesses. However, loss of labor-productivity and severe physiological impacts, including mortality, can occur at lower temperatures (Dunne et al., 2013; Leon & Bouchama, 2015). Raymond et al. (2020) showed that wet-bulb temperatures exceeding 35°C have already occurred and extreme wet-bulb temperatures have doubled in frequency, and Coffel et al. (2018) find that more frequent wet-bulb extremes are projected in several densely populated, vulnerable regions with continued warming.

Recent studies investigated spatiotemporal patterns and causes of changes in historical wet-bulb extremes over India (Mishra et al., 2020), Pakistan (Monteiro & Caballero, 2019), the USA (Raymond et al., 2017), and other climatologically hot and humid regions (Krakauer et al., 2020). However, the magnitude, seasonal timing, and frequency of humid-heat extremes, their spatial patterns, and societal exposure have not been quantified globally. Understanding spatiotemporal patterns and changes in humid-heat characteristics relative to dry-heat can reveal regions that face mounting human and ecosystem risks from extreme humid-heat which temperature-based metrics alone do not capture.

Using daily maximum temperatures from HadISD station data and high-resolution ERA5 reanalysis, we build a global climatology of the magnitude and seasonal timing of dry- and humid-heat extremes and examine how their characteristics have changed from 1979 to 2019. We also examine how their trends have contributed to changes in land-area and population exposure to both extremes. Our key aims include: (a) comparing global patterns of dry- and humid-heat extreme characteristics, (b) identifying differences in seasonal timing, and (c) illuminating consistencies and differences in recent trends. While our analyses are performed at the global-scale, our discussion focusses on regions with the hottest temperatures, strongest trends, strongest contrasts between dry- and humid-heat, or regions with high-population densities.

2. Data

We examine dry- and humid-heat (1979–2019) using ERA5 gridded hourly reanalysis (0.25° x 0.25°) (Copernicus Climate Change Service (C3S), 2017; Hersbach et al., 2019) and sub-daily HadISD observational station data version 3.1.1.202004p (Willett et al., 2014). While station data spatial coverage is incomplete, particularly in vulnerable global regions, ERA5 provides a spatially complete, physically consistent data set to study global patterns and recent trends. We use ERA5 dry-bulb temperature (DBT), dew-point temperature, and surface pressure, and HadISD DBT, specific humidity, elevation, and mean sea level pressure to calculate wet-bulb temperature (WBT). We use daily maximum temperatures instead of daily means to capture the most extreme values and because there are smaller differences between HadISD and ERA5 data in the daily maximum relative to the daily means (see Section S1 for HadISD station selection and bias control).

NASA Socioeconomic Data and Applications Center (SEDAC) gridded population and land-area are used to analyze changes in extreme heat exposure (CIESIN, 2018a, 2018b, 2018c). While population changes have affected global-population exposure to extremes, we use fixed, 2010 global-population and land-surface data to isolate climate change effects.

3. Methods

3.1. Wet-Bulb Temperature Definition

While other variables might characterize heat stress better, such as wet-bulb globe temperature which considers wind and solar radiation, these data are often limited in availability and quality, thus we use WBT. We use the Davies-Jones method (Davies-Jones, 2008) to calculate WBT (see Section S2 for the calculations) and the Buzan et al. (2015) implementation using the Kopp (2020) Matlab code. This method minimizes error at high-temperatures (Coffel et al., 2018, 2019; Raymond et al., 2020; Sherwood & Huber, 2010).

3.2. Extreme Heat Definitions and Metrics

The extreme heat threshold (*magnitude*) is the local 95th percentile over the 1981–2010 baseline. This definition identifies two extreme heat types: *dry-heat*, calculated using daily maximum DBT, and *humid-heat*, calculated using daily maximum WBT. We calculate these thresholds over the entire year instead of just summer to ensure consistency across the equator and for regions with weaker seasonal temperature and humidity cycles, such as the tropics, where extreme heat can occur year-round. Spatial trends are analyzed using the *summer-centric year* (Northern-Hemisphere: January–December, Southern-Hemisphere: July–June) rather than the calendar year to ensure that typical summer seasons in the Southern-Hemisphere extra-tropics are not split.

We define extreme dry- (humid-) heat days as any day exceeding the 95th percentile DBT (WBT) threshold. Extreme heat *frequency* is defined as the number of days above the corresponding dry- and humid-heat threshold, and *intensity* is the mean temperature on all extreme heat days. We calculate linear trends over 1979–2019 and estimate significance using the Mann-Kendall test. To characterize *seasonal timing* of extreme heat we find the month with the most heat days over 1979 to 2019 (peak-heat-month) and examine the temporal difference between the peak-heat-months for dry- and humid-heat. Lastly, we calculate the total number of months that experience at least five extreme heat days in the entire record as a *seasonality* measure. If this metric is high, heat events are not constrained to a particular time of year and seasonality is low, such as in the tropics. Conversely, if this metric is low, there is a strong seasonal cycle in temperatures and heat events are constrained to a particular time of year, such as at high-latitudes. While there are additional timing metrics for characterizing extreme heat impacts, the lack of a well-defined hot season in many tropical areas makes it challenging to define other globally consistent metrics for examining their global climatology. Measures of extreme heat timing tailored to a region's seasonality and vulnerabilities (e.g., timing of labor-intensive agricultural activities) are needed to more accurately assess regional and sectoral risks. Finally, we compare trends in annual 99th and 50th percentiles of daily maximum temperatures to determine whether extremes are changing at a different rate than the mean.

3.3. Population and Land Exposure

We examine extreme heat exposure using: (a) average number of heat extremes per-person or per-unit-land-area (Equations 1 and 2, respectively), and (b) total number of people or land-area simultaneously exposed to extreme heat per-day (Equations 3 and 4, respectively). These metrics are calculated as follows:

$$\text{hdpp}_i = \left(\sum_{y=-90}^{90} \sum_{x=0}^{360} \text{ndays}_{x,y,i} * \text{population}_{x,y} \right) / \text{total population} \quad (1)$$

where hdpp_i is population-weighted heat days for year i , $\text{ndays}_{x,y,i}$ is number of heat days for latitude y , longitude x , and year i , $\text{population}_{x,y}$ is population for the grid cell with latitude y , and longitude x , and total population is the total global-population.

$$\text{hdpkm}_i = \left(\sum_{y=-90}^{90} \sum_{x=0}^{360} \text{ndays}_{x,y,i} * \text{area}_{x,y} \right) / \text{total area} \quad (2)$$

where hdpkm_i is area-weighted heat days for year i (km^2), $\text{area}_{x,y}$ is square-kilometres of land in each grid cell, and total area is the total global land-area (excluding permanent ice and water).

$$\text{ppd}_{\text{mean},i} = \left(\sum_{y=-90}^{90} \sum_{x=0}^{360} \text{ndays}_{x,y,i} * \text{population}_{x,y} \right) / \text{total days}_i \quad (3)$$

where $\text{ppd}_{\text{mean},i}$ is annual average number of people simultaneously exposed to extreme heat per-day for year i , total days is number of days in year i .

$$\text{kmpd}_{\text{mean},i} = \left(\sum_{y=-90}^{90} \sum_{x=0}^{360} \text{ndays}_{x,y,i} * \text{area}_{x,y} \right) / \text{total days}_i \quad (4)$$

where $\text{kmpd}_{\text{mean},i}$ is average area simultaneously exposed to extreme heat per-day for year i .

Similar methods to Equations 3 and 4 are used to calculate maximum number of people ($\text{ppd}_{\text{max},i}$) and land-area ($\text{kmpd}_{\text{max},i}$) exposed to extreme dry- and humid-heat annually.

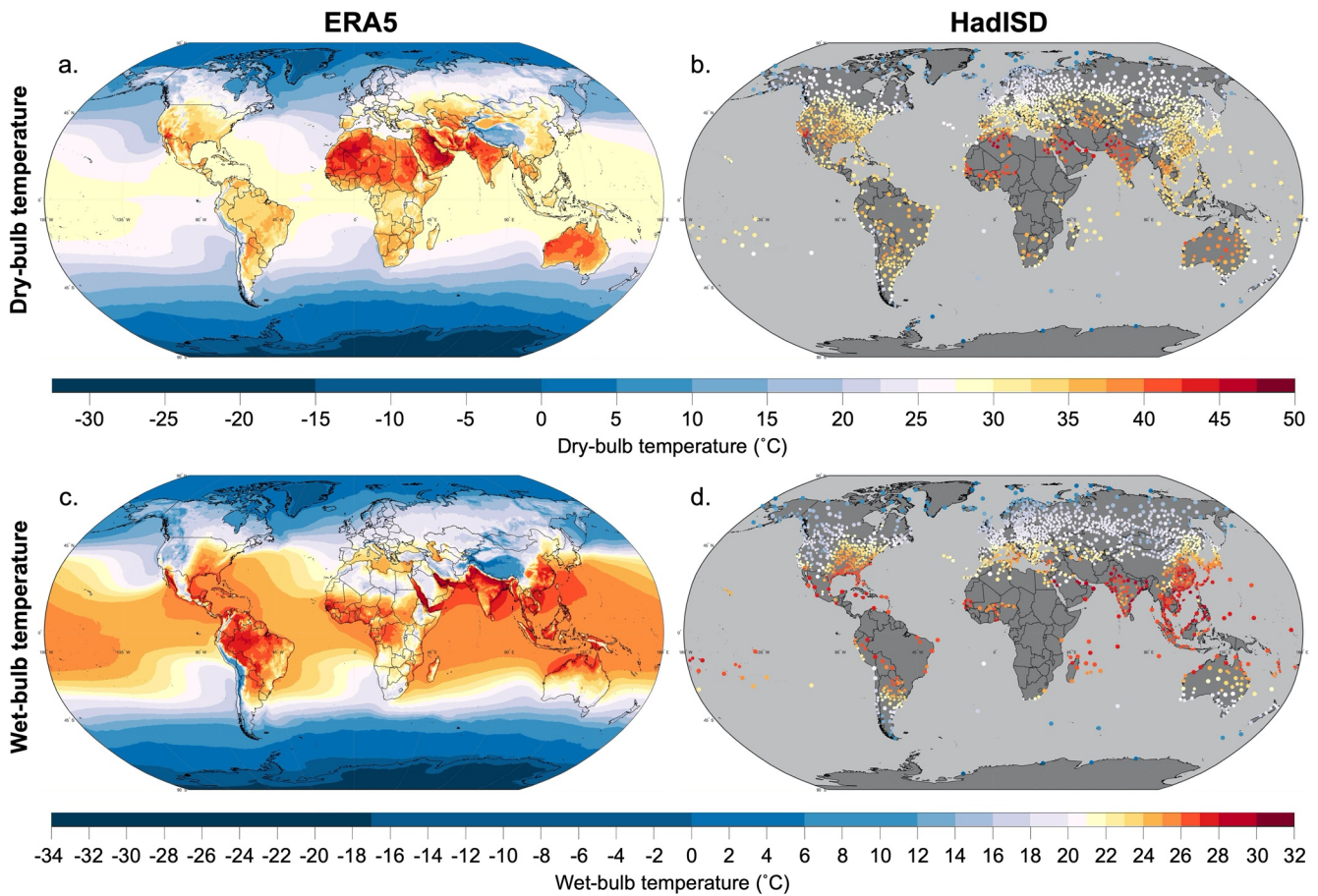


Figure 1. Extreme heat magnitude. Baseline (1981–2010) 95th percentile magnitude of (a and b) dry-bulb and (c and d) wet-bulb temperatures from ERA5 (left) and HadISD (right). To emphasize high values and their gradients in the hottest regions for each metric, we use different non-linear color scales for dry- and wet-bulb temperatures.

4. Results and Discussion

4.1. Extreme Heat Magnitude

The greatest differences between the spatial pattern of dry- and humid-heat magnitudes are associated with moisture availability differences (Figure 1). DBT extremes are hottest in the subtropics and desert regions, such as northern Africa, the Middle East, northwest South Asia, and Australia. In contrast, WBT extremes mainly peak in the tropics and subtropics; these locations correspond to humid, monsoonal areas, including South and Southeast Asia, the coastal Persian Gulf, and the western Amazon Basin (Matthews, 2018). Due to the high heat capacity of water, extreme DBT thresholds over the ocean are much cooler than those over nearby land regions, where there is limited moisture supply for evaporative cooling and consequently more sensible heating (Figure 1a). Conversely, this land-ocean contrast is less noticeable for WBT in the low-latitudes, particularly around South and Southeast Asia (Figure 1c). The lower land-ocean contrast for WBT in these regions where the environment is in convective quasi-equilibrium could be associated with their proximity to the warmest sea-surface temperatures in the Indo-Pacific Warm Pool, weak free tropospheric temperature gradient, and moisture advection from the ocean to land-areas via the regional monsoonal circulations.

While there are known underestimation biases due to spatiotemporal averaging for WBT extremes in the older-generation reanalyses—ERA-Interim (Dee et al., 2011; Raymond et al., 2020)—the spatial pattern of extreme heat magnitudes are largely consistent for ERA5 and HadISD (Figure 1), illustrating the suitability of ERA5 for analyzing the global-scale patterns of temperature extremes. Biases are likely to be largest over

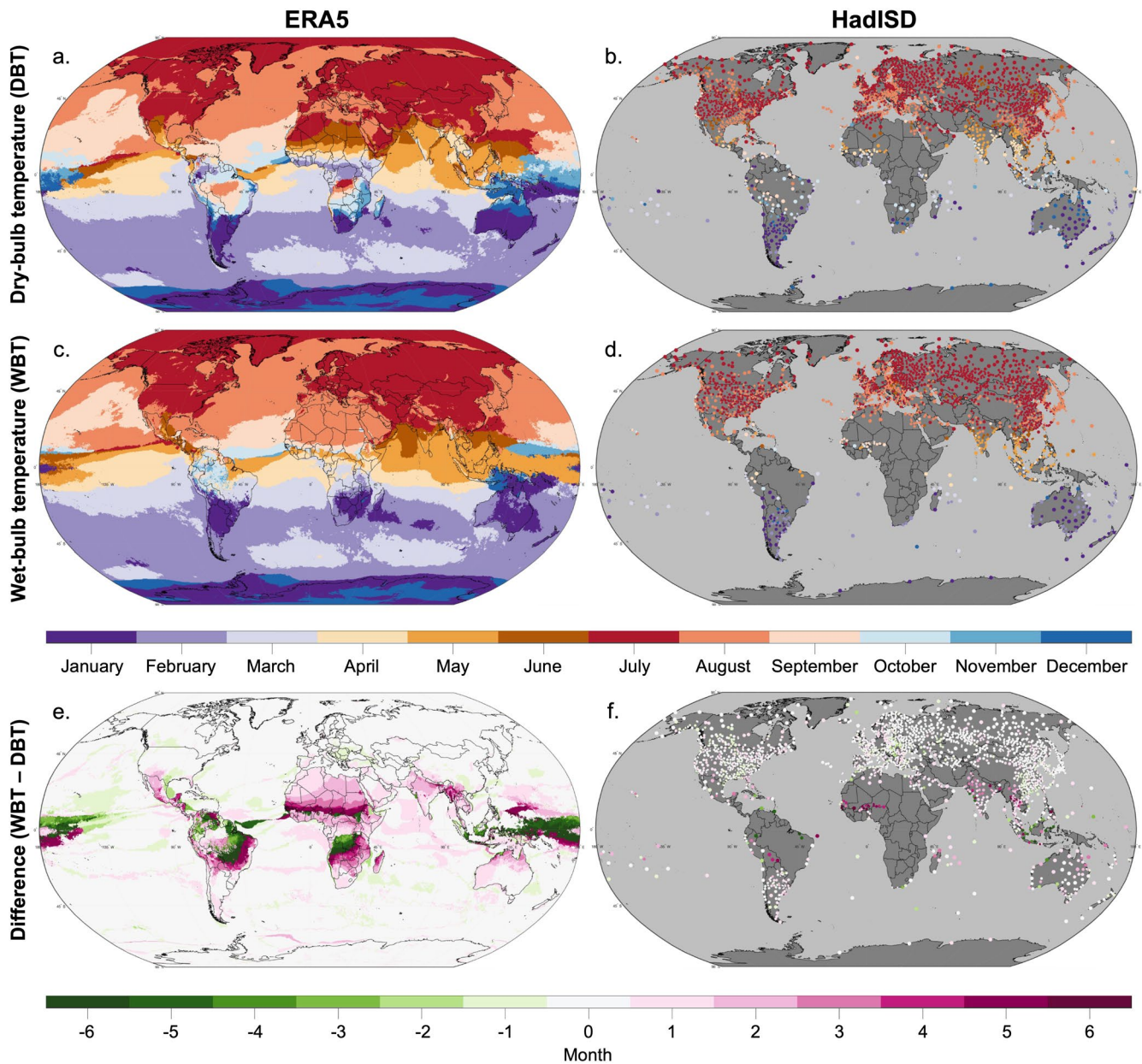


Figure 2. Seasonal timing of heat extremes. Month with the highest frequency of days with extreme (a and b) dry-bulb and (c and d) wet-bulb temperatures for ERA5 (left) and HadISD (right). (e and f) the difference between the peak month of humid-heat (c and d) and dry-heat extremes (a and b). Positive (negative) values, with pink (green) coloring, show where the peak wet-bulb month occurs after (before) that for dry-bulb.

landscapes with complex topography, land-sea contrasts, and low station-density, however ERA5's higher resolution should result in smaller biases than for ERA-Interim.

4.2. Extreme Heat Seasonal Timing

The seasonal timing of extreme heat events also shapes their impacts. For example, timing affects vegetation productivity (Butler & Huybers, 2015; Sun et al., 2018; Wang et al., 2016) and worker health impacts can be exacerbated if extreme heat coincides with outdoor labor activity, such as field preparation, sowing, and crop harvesting (De Lima et al., 2021; Spector et al., 2016; Tigchelaar et al., 2020). In the mid-to high-latitudes, there is a strong seasonal cycle where heat extremes occur most frequently during JJA (DJF) in the Northern (Southern) Hemisphere (Figures 2a–2d and S3), and extreme dry- and humid-heat days generally

occur during the same month (Figures 2e and 2f). Extreme heat frequency peaks earlier in the warm season over land than ocean due to the high heat capacity of water and resulting thermal inertia (Figures 2a and 2c). Conversely, the seasonality of extremes is weak across the tropics, where they can occur year-round (Figure S3), and the timing of peak dry- and humid-heat differ by multiple months (Figures 2e and 2f).

The largest differences in seasonal timing of dry- and humid-heat correspond to monsoonal or high annual rainfall regions across the low-latitudes (Wang & Ding, 2008; Zhang & Wang, 2008) with similar solar forcing throughout the year. In areas affected by the North African and North American monsoons, most dry-heat extremes tend to occur in May or June, whereas most humid-heat extremes occur in August (Figures 2a and 2c). Some monsoonal regions such as South Asia, experience the most humid-heat events in May before the typical monsoon season (June–September) or early in the monsoon season. The occurrence of humid-heat during the planting and early growing season (e.g., NFSM, n.d.), which is typically labor-intensive, puts agricultural workers at heightened risk of heat-related illnesses and can reduce work performance (Koteswara Rao et al., 2020).

4.3. Trends in Extreme Heat Frequency

Most of Europe, northern South America, Africa, the Arabian Peninsula, the Maritime Continent, and parts of the Pacific and Atlantic Oceans have significant positive trends in dry- and humid-heat frequencies (Figures 3a–3d). The strongest trends are in the tropics, where historical temperature variability is low, and in parts of the Arctic that have recently undergone substantial sea ice-loss (Screen et al., 2013). Several regions that experience positive trends in humid-heat frequency (Figure 3c) correspond to areas where the 95th percentile already exceeds dangerous WBTs ($\geq 27^{\circ}\text{C}$; Krakauer et al., 2020), such as northern India, parts of Southeast Asia, and northern Bolivia/western Brazil (Figure 1c). Extreme heat frequency has increased by up to 35 additional dry-heat days and 28 humid-heat days per-decade for ERA5 (Figures 3a and 3c). HadISD shows a similar pattern of trends although with larger magnitudes in some regions (Figures 3b and 3d).

Dry- and humid-heat frequency trends are consistent in sign and significance over most regions (Figures 3e and 3f). Further, positive extreme heat frequency trends are associated with increases in mean intensity (Figures S4a and S4b) and an expansion of the number of months and the number of pentads with extreme heat occurrences (Figures S4c–S4f). While extreme heat frequency trends for ERA5 and HadISD differ by an average of 3.0 (3.7) days per-decade for dry-heat (humid-heat; Section S1), the spatial pattern of trends compares well over most land regions, with the greatest differences occurring over the tropics (e.g., Indonesia) and mountainous regions (e.g., the Andes; Figures S2a and S2b).

While dry- and humid-heat frequency trends are largely consistent, a few regions show divergent trends (Figures 3e and 3f). For example, humid-heat frequency trends are strongest over highly populous regions in South and Southeast Asia where changes in dry-heat frequency are small or non-significant. Since a large fraction of land-area in these regions is croplands (Ramankutty et al., 2010), and the timing of high irrigation rates over India coincide with the warmest temperatures, increasing irrigation intensity could be increasing humidity and consequently extreme humid-heat (e.g., Krakauer et al., 2020; Mishra et al., 2020) while cooling the land-surface via increased latent-heat fluxes (Singh et al., 2018). Increased humid-heat frequency over India also corresponds to areas with recent increases in annual rainfall and surface specific humidity (Hartmann et al., 2013). Contrastingly, significant increases in dry-heat days but not humid-heat days over eastern China (Figures 3a and 3c), where rainfall and surface specific humidity have declined (Hartmann et al., 2013), indicates that humidity changes are likely influencing the diverging trends in dry- and humid-heat extremes. The contributions of factors including land-use/land-cover change, aerosol-related cooling, and precipitation changes (Myhre et al., 2013) to diverging dry- and humid-heat trends are yet to be evaluated.

4.4. Extreme Heat Exposure

Changing extreme heat frequencies contributed to significant increases in the *mean* exposure of the global-population and land-surface to locally defined heat extremes (Figures 3g, 3h, and S5). Comparing population-weighted and area-weighted extreme heat frequency trends highlights differences in the areas affected by these extremes (Figures 3g and 3h). *Mean* humid-heat exposure increased by ~ 3.6 days per-unit-land-area

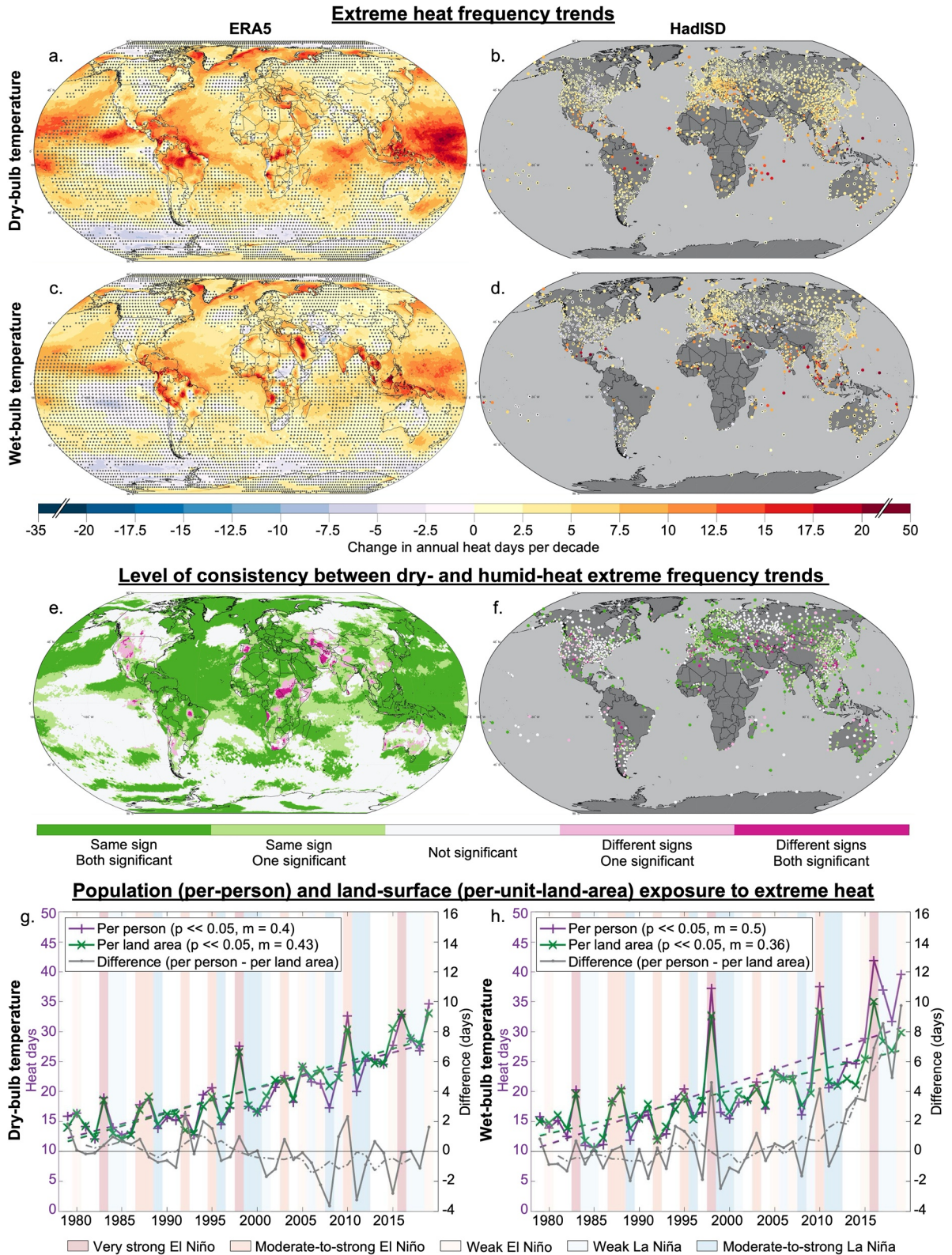


Figure 3.

per-decade, but by ~ 5.0 days per-person per-decade, illustrating that humid-heat frequency trends disproportionately affected populated regions (Figure 3h). Conversely, *mean* dry-heat day trends are of similar magnitude per-person and per-unit-land-area (~ 4.0 and ~ 4.3 additional days per-decade, respectively), thus dry-heat has a more uniform imprint across the world (Figure 3g). Further, the daily *maximum* number of people simultaneously affected by humid-heat (average annual maximum of ~ 2.0 billion people between 1979 and 2019) is higher than that for dry-heat (~ 1.5 billion people; Figure S5c). A similar pattern is found for land-area (Figure S5d).

While both dry- and humid-heat have become more frequent and affected more people and land (Figures S5a and S5b), the global-population has become increasingly exposed to humid-heat at a faster rate than to dry-heat (Figures S5a and S5c), driven by high humid-heat frequency trends over highly populated regions, including parts of Asia (Figures 3c and 3d). The stronger overall land exposure trends for dry-heat (~ 4.3 days per-decade) compared to humid-heat (~ 3.6 days per-decade) further suggests that humid-heat predominantly affected populated regions (Figures S5b and S5d), consistent with recent theoretical (Matthews, 2018) and modeling (Coffel et al., 2018) work. Since we do not consider population change, and populations have predominantly increased in regions with increasing humid-heat frequency (e.g., India), our findings likely constitute conservative estimates of population exposure changes. These findings highlight the importance of considering humidity when assessing the increasing risks of extreme heat on human-health in a changing climate.

The 1997–1998, 2009–2010, and 2015–2016 El Niños are associated with the highest annual-average land exposure to humid-heat (Figures 3h and S5b; NOAA, 2021). Land exposure for dry-heat, and population exposure for both extremes, are also high for these years (Figures 3g, 3h, S5a, and S5b), but lower than for humid-heat population exposure (Figures S5a and S5f), suggesting that El Niños might disproportionately exacerbate WBT in densely populated areas. However, the long-term humid-heat trend is not solely driven by these events (Figure S6b). Similar, albeit weaker annual trends result when 1997–98, 2009–2010, and 2015–2016 are removed—decrease from 0.40 to 0.36 for dry-heat days per-person, and 0.50 to 0.43 for humid-heat days per-person (Figures 3g, 3h, and S6)—further supporting our finding that population exposure to humid-heat has the strongest trend (Figures 3g, 3h, and S6). Further, while the differences between population and land-area exposure to humid-heat are most positive (negative) during El Niños (La Niñas) from 1979 to 2011 (Figure 3h), these differences are positive every year since 2012, even during the weak La Niñas in 2016–2017 and 2017–2018. Although there is no noticeable trend in the difference between per-person and per-unit-land-area exposure to humid-heat prior to 2010 (Figure 3h), we find an indication of an emerging positive trend in the past decade where this difference is consistently positive and has its highest magnitude in recent years.

A composite of the spatial patterns of heat day frequencies during the 1997–1998, 2009–2010, and 2015–2016 El Niños (Figures S7a–S7f) indicates a higher frequency of dry-heat over northern South America, Africa, Europe, and the Maritime Continent (Figure S7g), and extreme humid-heat over northern South America, Africa, the Middle East, India, and Southeast Asia (Figure S7h). The higher-population exposure to humid-heat relative to dry-heat is due to higher humid-heat day frequencies over densely populated regions, such as India, Bangladesh, and Nigeria (all three years), and additionally Southeast China (1998, 2016), and Southeast Asia (2010, 2016; Figures S8a–S8d). The composite of all historical strong and very strong El Niño events since 1979 shows a much weaker pattern (Figures S7i, S7j, and S8e) likely because every El Niño is distinct and has different spatial features and varying regional impacts (e.g., Johnson & Kosaka, 2016; van Rensch et al., 2019). Further, El Niños in the past decade act on a warmer background climate than previous events, making it challenging to identify consistent regional signals of El Niños over the

Figure 3. Extreme heat frequency and exposure trends. Trends in the number of extreme (a and b) dry- and (c and d) humid-heat days per-decade for ERA5 (left) and HadISD (right). Stippling indicates trends that are *not* significant. (e and f) Level of consistency between trends in dry- and humid-heat extremes. (g and h) the number of extreme heat days per-person (purple “+” markers) and per-unit-land-area (km², green “x” markers) for dry- and humid-heat (left y-axis). Dashed (dotted) lines show linear trends that are significant (not significant). *m* indicates trend magnitude. Gray lines with “.” markers show differences between heat days per-person and heat days per-unit-land-area (right y-axis). Dash-dot lines show 5-year moving average for these differences. Colored bars show El Niño strength, determined using the Oceanic Niño Index (ONI, NOAA, 2021); very strong El Niño (red, ONI > 2), moderate-to-strong El Niño (dark pink, 1 < ONI < 2), weak El Niño (light pink, 0.5 < ONI < 1), weak La Niña (light blue, -1 < ONI < -0.5), and moderate-to-strong La Niña (dark blue, ONI < -1). Black horizontal line shows where right y-axis equals zero. Trend significance in this figure is determined using the Mann-Kendall test (Fatichi, 2020) at the 95% confidence level.

limited historical record (Figures S7 and S8). Therefore, while El Niños are known to affect DBT (Arblaster & Alexander, 2012) and WBT (Raymond et al., 2020), diagnosing the regional teleconnections of El Niño on humid-heat requires large-ensemble simulations to examine the influence of different El Niño flavors and warming on the teleconnections. Our findings demonstrate the need to more thoroughly examine the relationship between the spatial patterns of extreme heat with ENSO and other climate modes.

4.5. Changing Temperature Distributions

In some regions, climate change is altering the shape of temperature distributions beyond a simple shift in the mean. Stronger changes in the tails of the distribution compared to the mean have different implications for human and ecosystem health. Here, we compare trends in the median and 99th percentile (Figure S9) to determine whether (a) temperature distributions are changing shape, and (b) the hottest extremes are getting hotter. ERA5 and HadISD trends are largely consistent, except over western Russia (Figures S9 and S10).

Many regions show stronger median DBT trends relative to the 99th percentile including the Arctic, eastern North America, Asia, northern Africa, and northern Australia (Figures S9a, S9c, and S9e). However, over land-areas such as South America, western North America, Europe, and southeastern Australia, the 99th percentile DBT has increased more than the median. In addition to the creeping changes associated with mean warming, such larger changes in heat extremes could be driven by diverse drivers including increases in atmospheric blocking (e.g., Horton et al., 2015; Sousa et al., 2018), and increased soil moisture deficits (Donat et al., 2017; Hirschi et al., 2011). Differences between the 99th percentile and median trends likely reflect the influence of different drivers in different seasons. For example, greater trends in the 99th percentile of DBT off eastern Canada and the Barents and Kara Seas are associated with regions experiencing summer sea-ice loss (Screen et al., 2013), whereas mean DBTs during winter, spring, and autumn over the majority of the Arctic (65°–90°N) have increased at a greater rate than for summer (Johannessen et al., 2016; Figure S9).

The 99th percentile of WBT tends to increase at a similar or weaker rate than the median over much of the global land-area (Figures S9b, S9d, and S9f). Several regions show significant positive trends in the median WBT (Figure S9d) without corresponding significant changes in the 99th percentile (Figure S9b), including much of Asia. Conversely, parts of Africa, the Americas, and the Middle East, show stronger 99th percentile trends compared to the median. Compared to dry-heat, more regions show negative or non-significant humid-heat trends (Figures S9a–S9d), suggesting relative drying not cooling is responsible for these changes. These findings are consistent with the expectation of WBT increasing slower than DBT with warming—approximately 0.9°C of WBT per 1.0°C of DBT—with constant relative humidity (Buzan & Huber, 2020). With global warming, relative humidity is expected to decrease (Buzan & Huber, 2020; Byrne & O’Gorman, 2013, 2018), which might further reduce the rate of increase of WBT relative to DBT.

5. Conclusions and Implications

We characterize and compare dry- and humid-heat extremes on a global-scale using ERA5 reanalysis and HadISD station data and assess changes in exposure. While extreme DBT alone has implications for human-health, infrastructure damage, and crop loss, WBT more closely captures the effect of climate on human-health. We identify a greater increase in population exposure to humid-heat as compared to dry-heat, emphasizing the importance of understanding humidity changes in a warming world. We show that most of Europe, northern South America, Africa, the Arabian Peninsula, the Maritime Continent, and Northern-Hemisphere oceans (representing ~27% of global area) have experienced statistically significant increases in both dry- and humid-heat extremes. Several regions also experience divergent trends in these extremes. For instance, most of South Asia experiences increases in humid-heat extremes despite non-significant changes in dry-heat.

Our research builds on previous studies that identified humid-heat as a risk to human-health (e.g., Raymond et al., 2020; Sherwood & Huber, 2010). We link together existing threads of humid-heat research by showing that the newly available high-resolution ERA5 reanalysis compares well in regions with high station density and low topographic complexity. Our study extends this research to provide information on

changes in dry- and humid-heat extremes for understudied regions of Africa and South America, where reliable station data are limited. We also provide novel findings quantifying the seasonal timing of extremes, including identifying a difference of several months between dry- and humid-heat in monsoonal and tropical regions, which is not observed in the extra-tropics. Further, we show that strong increases in extreme heat frequency are accompanied by an expansion of the number of months during which they occur.

While we examine extreme heat trends on a global-scale, understanding the influence of urban development on observed trends could provide additional insights. Previous research has examined the urban heat island effect during extreme dry-heat in temperate cities (e.g., Li & Bou-Zeid, 2013; Rogers et al., 2019; Scott et al., 2018), but there is limited research examining the effect of heat extremes in tropical cities (e.g., Chew et al., 2021). We also highlight limits to adaptation. With rising WBTs, including over areas already approaching the survivability limit (35°C), manual, labor-intensive outdoor work such as agricultural activities, construction, and pulled- or cycle-powered rickshaw transport could effectively become infeasible during the hot parts of the day for much of the year.

Given the higher-population exposure to humid-heat and its projected increases, particularly in vulnerable areas, our findings emphasize the need to better understand societal impacts (Coffel et al., 2018; Raymond et al., 2020) by considering the timing of location-specific human activities, demographics, and socio-economic factors that enhance vulnerability to heat stress, as well as incorporating additional physical factors such as solar radiation and wind. This understanding is of heightened importance to communities with one or more of the following risk factors: (a) vulnerable workers directly exposed to extreme heat (such as farm workers or urban outdoor laborers), (b) limited access to air conditioning, electricity, community cooling centers, health and emergency medical services, (c) inadequate extreme-heat warning systems, (d) people without housing, and (e) older-populations and those with certain health conditions. While it is imperative that we reduce global carbon emissions to avoid the worst impacts of climate change, addressing the above socio-economic factors and infrastructure issues (e.g., Fouillet et al., 2008) through policy, adaptation measures, or financial aid can help reduce the impacts of committed climate change.

Conflict of Interest

The authors declare no conflicts of interest relevant to this study.

Data Availability Statement

ERA5 data for the 2-m level are available at <https://cds.climate.copernicus.eu/cdsapp#!/dataset/reanalysis-era5-single-levels?tab=form>. ERA5 data for the 850-hPa level are available at <https://cds.climate.copernicus.eu/cdsapp#!/dataset/reanalysis-era5-pressure-levels?tab=form>. HadISD data are available at <https://www.metoffice.gov.uk/hadobs/hadisd/index.html>. SEDAC population data are available at <https://sedac.ciesin.columbia.edu/data/set/gpw-v4-basic-demographic-characteristics-rev11/data-download> and land data are available at <https://sedac.ciesin.columbia.edu/data/set/gpw-v4-land-water-area-rev11/data-download>. ONI data are available at https://origin.cpc.ncep.noaa.gov/products/analysis_monitoring/ensostuff/ONI_v5.php. ERA5 analyses were run on Washington State University's high-performance computing cluster, Kamiak. The authors used the following Matlab packages: the Climate Data Toolbox for Matlab (Greene et al., 2019), and the Mann-Kendall Test package (Fatichi, 2020).

Acknowledgments

The authors acknowledge the use of ERA5 reanalysis as a key data set used in the manuscript. Funding for C.D.W. Rogers and D. Singh provided by grant NSF - AGS - 1934383. Funding for M. Ting, C. Li, K. Kornhuber, and R.M. Horton provided by grant NSF - AGS - 1934358. E.D. Coffel's funding provided by Syracuse University Appleby-Mosher Grant. C. Raymond's portion of the work was carried out at the Jet Propulsion Laboratory, California Institute of Technology, under a contract with the National Aeronautics and Space Administration.

References

- Arblaster, J. M., & Alexander, L. V. (2012). The impact of the El Niño-Southern Oscillation on maximum temperature extremes. *Geophysical Research Letters*, 39(20), 2–6. <https://doi.org/10.1029/2012GL053409>
- Butler, E. E., & Huybers, P. (2015). Variations in the sensitivity of US maize yield to extreme temperatures by region and growth phase. *Environmental Research Letters*, 10(3), 034009. <https://doi.org/10.1088/1748-9326/10/3/034009>
- Buzan, J. R., & Huber, M. (2020). Moist heat stress on a hotter Earth. *Annual Review of Earth and Planetary Sciences*, 48, 623–655. <https://doi.org/10.1146/annurev-earth-053018-060100>
- Buzan, J. R., Oleson, K., & Huber, M. (2015). Implementation and comparison of a suite of heat stress metrics within the Community Land Model version 4.5. *Geoscientific Model Development*, 8(2), 151–170. <https://doi.org/10.5194/gmd-8-151-2015>
- Byrne, M. P., & O'Gorman, P. A. (2013). Link between land-ocean warming contrast and surface relative humidities in simulations with coupled climate models. *Geophysical Research Letters*, 40, 5223–5227. <https://doi.org/10.1002/grl.50971>

- Byrne, M. P., & O'Gorman, P. A. (2018). Trends in continental temperature and humidity directly linked to ocean warming. *Proceedings of the National Academy of Sciences of the United States of America*, 115(19), 4863–4868. <https://doi.org/10.1073/pnas.1722312115>
- Chew, L. W., Liu, X., Li, X. X., & Norford, L. K. (2021). Interaction between heat wave and urban heat island: A case study in a tropical coastal city, Singapore. *Atmospheric Research*, 247, 105134. <https://doi.org/10.1016/j.atmosres.2020.105134>
- CIESIN - Center for International Earth Science Information Network - Columbia University. (2018a). *Documentation for the gridded population of the World, version 4 (GPWv4)* (Revision 11 data sets). <https://doi.org/10.7927/H45Q4T5F>
- CIESIN - Center for International Earth Science Information Network - Columbia University. (2018b). *Gridded population of the World, version 4 (GPWv4): Basic demographic characteristics, revision 11*. <https://doi.org/10.7927/H46M34XX>
- CIESIN - Center for International Earth Science Information Network - Columbia University. (2018c). *Gridded population of the World, version 4 (GPWv4): Land and water area, revision 11*. <https://doi.org/10.7927/H4Z60M4Z>
- Coffel, E. D., Horton, R. M., & De Sherbinin, A. (2018). Temperature and humidity based projections of a rapid rise in global heat stress exposure during the 21st century. *Environmental Research Letters*, 13(1). <https://doi.org/10.1088/1748-9326/aaa00e>
- Coffel, E. D., Horton, R. M., Winter, J. M., & Mankin, J. S. (2019). Nonlinear increases in extreme temperatures paradoxically dampen increases in extreme humid-heat. *Environmental Research Letters*, 14(8), 084003. <https://doi.org/10.1088/1748-9326/ab28b7>
- Copernicus Climate Change Service (C3S). (2017). *ERA5: Fifth generation of ECMWF atmospheric reanalyses of the global climate*. Copernicus Climate Change Service Climate Data Store (CDS). Retrieved from <https://cds.climate.copernicus.eu/cdsapp#!/home>
- Davies-Jones, R. (2008). An efficient and accurate method for computing the wet-bulb temperature along pseudoadiabats. *Monthly Weather Review*, 136(7), 2764–2785. <https://doi.org/10.1175/2007MWR2224.1>
- Dee, D. P., Uppala, S. M., Simmons, A. J., Berrisford, P., Poli, P., Kobayashi, S., et al. (2011). The ERA-Interim reanalysis: Configuration and performance of the data assimilation system. *Quarterly Journal of the Royal Meteorological Society*, 137(656), 553–597. <https://doi.org/10.1002/qj.828>
- De Lima, C. Z., Buzan, J. R., Moore, F. C., Baldos, U. L. C., Huber, M., & Hertel, T. W. (2021). Heat stress on agricultural workers exacerbates crop impacts of climate change. *Environmental Research Letters*, 16(4), 044020. <https://doi.org/10.1088/1748-9326/abeb9f>
- Donat, M. G., Pitman, A. J., & Seneviratne, S. I. (2017). Regional warming of hot extremes accelerated by surface energy fluxes. *Geophysical Research Letters*, 44(13), 7011–7019. <https://doi.org/10.1002/2017GL073733>
- Dunne, J. P., Stouffer, R. J., & John, J. G. (2013). Reductions in labour capacity from heat stress under climate warming. *Nature Climate Change*, 3(6), 563–566. <https://doi.org/10.1038/nclimate1827>
- Fatichi, S. (2020). *Mann-Kendall test*. Retrieved from <https://www.mathworks.com/matlabcentral/fileexchange/25531-mann-kendall-test>
- Fouillet, A., Rey, G., Wagner, V., Laaidi, K., Empereur-Bissonnet, P., Le Tertre, A., et al. (2008). Has the impact of heat waves on mortality changed in France since the European heat wave of summer 2003? A study of the 2006 heat wave. *International Journal of Epidemiology*, 37(2), 309–317. <https://doi.org/10.1093/ije/dym253>
- Greene, C. A., Thirumalai, K., Kearney, K. A., Delgado, J. M., Schwanghart, W., Wolfenbarger, N. S., et al. (2019). The climate data toolbox for MATLAB. *Geochemistry, Geophysics, Geosystems*, 20(7), 3774–3781. <https://doi.org/10.1029/2019GC008392>
- Hanna, E. G., & Tait, P. W. (2015). Limitations to thermoregulation and acclimatization challenge human adaptation to global warming. *International Journal of Environmental Research and Public Health*, 12(7), 8034–8074. <https://doi.org/10.3390/ijerph12078034>
- Hartmann, D. L., Klein Tank, A. M. G., Rusticucci, M., Alexander, L. V., Brönnimann, S., Charabi, Y., et al. (2013). Observations: Atmosphere and surface. In Stocker, T. F., Qin, D., Plattner, G.-K., Tignor, M., Allen, S. K., Boschung, J., et al. (Eds.), *Climate change 2013: The physical science basis. Contribution of working group I to the fifth assessment report of the intergovernmental panel on climate change* (pp. 159–254). Cambridge, United Kingdom and New York, NY: Cambridge University Press. <https://doi.org/10.1017/CBO9781107415324.008>
- Hersbach, H., Bell, B., Berrisford, P., Horányi, A., Sabater, J. M., Nicolas, J., et al. (2019). Global reanalysis: Goodbye ERA-Interim, hello ERA5. *ECMWF Newsletter*, 159, 17–24. <https://doi.org/10.21957/vf291hehd7>
- Hirschi, M., Seneviratne, S. I., Alexandrov, V., Boberg, F., Boroneant, C., Christensen, O. B., et al. (2011). Observational evidence for soil-moisture impact on hot extremes in southeastern Europe. *Nature Geoscience*, 4, 17–21. <https://doi.org/10.1038/ngeo1032>
- Hoegh-Guldberg, O., Jacob, D., Taylor, M., Bindi, M., Brown, S., Camilloni, I., et al. (2018). Impacts of 1.5°C global warming on natural and human systems. In Masson-Delmotte, V., Zhai, P., Pörtner, H.-O., Roberts, D., Skea, J., Shukla, P. R., et al. (Eds.), *Global warming of 1.5°C. An IPCC special report on the impacts of global warming of 1.5°C above pre-industrial levels and related global greenhouse gas emission pathways, in the context of strengthening the global response to the threat of climate change* (pp. 175–311). Retrieved from <https://www.ipcc.ch/sr15/chapter/chapter-3/>
- Horton, D. E., Johnson, N. C., Singh, D., Swain, D. L., Rajaratnam, B., & Diffenbaugh, N. S. (2015). Contribution of changes in atmospheric circulation patterns to extreme temperature trends. *Nature*, 522(7557), 465–469. <https://doi.org/10.1038/nature14550>
- IPCC. (2013). Summary for policymakers. In Stocker, T. F., Qin, D., Plattner, G.-K., Tignor, M., Allen, S. K., Boschung, J., et al. (Eds.), *Climate change 2013: The physical science basis. Contribution of working group I to the fifth assessment report of the intergovernmental panel on climate change*. Cambridge, United Kingdom and New York, NY: Cambridge University Press.
- Johannessen, O. M., Kuzmina, S. I., Bobylev, L. P., & Miles, M. W. (2016). Surface air temperature variability and trends in the Arctic: New amplification assessment and regionalisation. *Tellus, Series A: Dynamic Meteorology and Oceanography*, 68(1), 28234. <https://doi.org/10.3402/tellusa.v68.28234>
- Johnson, N. C., & Kosaka, Y. (2016). The impact of eastern equatorial Pacific convection on the diversity of boreal winter El Niño teleconnection patterns. *Climate Dynamics*, 47(12), 3737–3765. <https://doi.org/10.1007/s00382-016-3039-1>
- Kopp, B. (2020). *WetBulb.m*. Retrieved from <https://github.com/bobkopp/WetBulb.m>
- Kornhuber, K., Coumou, D., Vogel, E., Lesk, C., Donges, J. F., Lehmann, J., & Horton, R. M. (2020). Amplified Rossby waves enhance risk of concurrent heatwaves in major breadbasket regions. *Nature Climate Change*, 10(1), 48–53. <https://doi.org/10.1038/s41558-019-0637-z>
- Koteswara Rao, K., Lakshmi Kumar, T. V., Kulkarni, A., Ho, C. H., Mahendranath, B., Desamsetti, S., et al. (2020). Projections of heat stress and associated work performance over India in response to global warming. *Scientific Reports*, 10(1), 1–14. <https://doi.org/10.1038/s41598-020-73245-3>
- Krakauer, N. Y., Cook, B. I., & Puma, M. J. (2020). Effect of irrigation on humid heat extremes. *Environmental Research Letters*, 15(9), 094010. <https://doi.org/10.1088/1748-9326/ab9ecf>
- Leon, L. R., & Bouchama, A. (2015). Heat stroke. *Comprehensive Physiology*, 5(2), 611–647. <https://doi.org/10.1002/cphy.c140017>
- Li, D., & Bou-Zeid, E. (2013). Synergistic interactions between Urban Heat islands and heat waves: The impact in cities is larger than the sum of its parts. *Journal of Applied Meteorology and Climatology*, 52(9), 2051–2064. <https://doi.org/10.1175/JAMC-D-13-02.1>
- Matthews, T. (2018). Humid heat and climate change. *Progress in Physical Geography: Earth and Environment*, 42(3), 391–405. <https://doi.org/10.1177/0309133318776490>

- McEvoy, D., Ahmed, I., & Mullett, J. (2012). The impact of the 2009 heat wave on Melbourne's critical infrastructure. *Local Environment*, 17(8), 783–796. <https://doi.org/10.1080/13549839.2012.678320>
- Meehl, G. A., & Tebaldi, C. (2004). More intense, more frequent, and longer lasting heat waves in the 21st century. *Science*, 305(5686), 994–997. <https://doi.org/10.1126/science.1098704>
- Mishra, V., Ambika, A. K., Asoka, A., Aadhar, S., Buzan, J., Kumar, R., & Huber, M. (2020). Moist heat stress extremes in India enhanced by irrigation. *Nature Geoscience*, 13(11), 722–728. <https://doi.org/10.1038/s41561-020-00650-8>
- Monteiro, J. M., & Caballero, R. (2019). Characterization of extreme wet-bulb temperature events in southern Pakistan. *Geophysical Research Letters*, 46(17–18), 10659–10668. <https://doi.org/10.1029/2019GL084711>
- Myhre, G., Shindell, D., Bréon, F.-M., Collins, W., Fuglestedt, J., Huang, J., et al. (2013). Anthropogenic and natural radiative forcing. In Stocker, T. F., Qin, D., Plattner, G.-K., Tignor, M., Allen, S. K., Boschung, J., et al. (Eds.), *Climate change 2013: The physical science basis. Contribution of working group I to the fifth assessment report of the intergovernmental panel on climate change* (pp. 659–740). Cambridge University Press, Cambridge, United Kingdom and New York, NY. <https://doi.org/10.1017/CBO9781107415324.018>
- NFSM. (n.d.). *Crop calendar of NFSM crops*. Retrieved from <https://nfsm.gov.in/nfms/rpt/calenderreport.aspx>
- NOAA. (2021). *Cold & warm episodes by season*. Retrieved from https://origin.cpc.ncep.noaa.gov/products/analysis_monitoring/ensostuff/ONI_v5.php
- Perkins, S. E., Alexander, L. V., & Nairn, J. R. (2012). Increasing frequency, intensity and duration of observed global heatwaves and warm spells. *Geophysical Research Letters*, 39(20), 1–5. <https://doi.org/10.1029/2012GL053361>
- Perkins-Kirkpatrick, S. E., & Lewis, S. C. (2020). Increasing trends in regional heatwaves. *Nature Communications*, 11, 3357. <https://doi.org/10.1038/s41467-020-16970-7>
- Ramankutty, N., Evan, A. T., Monfreda, C., & Foley, J. A. (2010). *Global agricultural lands*. Croplands. <https://doi.org/10.7927/H4C8276G>
- Raymond, C., Matthews, T., & Horton, R. M. (2020). The emergence of heat and humidity too severe for human tolerance. *Science Advances*, 6(19). <https://doi.org/10.1126/sciadv.aaw1838>
- Raymond, C., Singh, D., & Horton, R. M. (2017). Spatiotemporal patterns and synoptics of extreme wet-bulb temperature in the contiguous United States. *Journal of Geophysical Research: Atmospheres*, 122(24), 13108–13124. <https://doi.org/10.1002/2017JD027140>
- Rogers, C. D. W., Gallant, A. J. E., & Tapper, N. J. (2019). Is the urban heat island exacerbated during heatwaves in southern Australian cities? *Theoretical and Applied Climatology*, 137(1–2), 441–457. <https://doi.org/10.1007/s00704-018-2599-x>
- Russo, S., Dosio, A., Graversen, R. G., Sillmann, J., Carrao, H., Dunbar, M. B., et al. (2014). Magnitude of extreme heat waves in present climate and their projection in a warming world. *Journal of Geophysical Research Atmospheres*, 119(22), 12500–12512. <https://doi.org/10.1002/2014JD022098>
- Scott, A. A., Waugh, D. W., & Zaitchik, B. F. (2018). Reduced Urban Heat Island intensity under warmer conditions. *Environmental Research Letters*, 13, 064003. <https://doi.org/10.1088/1748-9326/aab6dc>
- Screen, J. A., Simmonds, I., Deser, C., & Tomas, R. (2013). The atmospheric response to three decades of observed arctic sea ice loss. *Journal of Climate*, 26(4), 1230–1248. <https://doi.org/10.1175/JCLI-D-12-00063.1>
- Sherwood, S. C., & Huber, M. (2010). An adaptability limit to climate change due to heat stress. *Proceedings of the National Academy of Sciences of the United States of America*, 107(21), 9552–9555. <https://doi.org/10.1073/pnas.0913352107>
- Singh, D., McDermid, S. P., Cook, B. I., Puma, M. J., Nazarenko, L., & Kelley, M. (2018). Distinct influences of land cover and land management on seasonal climate. *Journal of Geophysical Research: Atmospheres*, 123(21), 12017–12039. <https://doi.org/10.1029/2018JD028874>
- Sousa, P. M., Trigo, R. M., Barriopedro, D., Soares, P. M. M., & Santos, J. A. (2018). European temperature responses to blocking and ridge regional patterns. *Climate Dynamics*, 50(1), 457–477. <https://doi.org/10.1007/s00382-017-3620-2>
- Spector, J. T., Bonauto, D. K., Sheppard, L., Busch-Isaksen, T., Calkins, M., Adams, D., et al. (2016). A case-crossover study of heat exposure and injury risk in outdoor agricultural workers. *PLoS ONE*, 11(10), 30–33. <https://doi.org/10.1371/journal.pone.0164498>
- Sun, T., Hasegawa, T., Tang, L., Wang, W., Zhou, J., Liu, L., et al. (2018). Stage-dependent temperature sensitivity function predicts seed-setting rates under short-term extreme heat stress in rice. *Agricultural and Forest Meteorology*, 256–257, 196–206. <https://doi.org/10.1016/j.agrformet.2018.03.006>
- Tigchelaar, M., Battisti, D. S., & Spector, J. T. (2020). Work adaptations insufficient to address growing heat risk for U.S. agricultural workers. *Environmental Research Letters*, 15(9), 094035. <https://doi.org/10.1088/1748-9326/ab86f4>
- van der Velde, M., Wriedt, G., & Bouraoui, F. (2010). Estimating irrigation use and effects on maize yield during the 2003 heatwave in France. *Agriculture, Ecosystems and Environment*, 135(1–2), 90–97. <https://doi.org/10.1016/j.agee.2009.08.017>
- van Rensch, P., Arblaster, J., Gallant, A. J. E., Cai, W., Nicholls, N., & Durack, P. J. (2019). Mechanisms causing east Australian spring rainfall differences between three strong El Niño events. *Climate Dynamics*, 53(5–6), 3641–3659. <https://doi.org/10.1007/s00382-019-04732-1>
- Wang, B., & Ding, Q. (2008). Global monsoon: Dominant mode of annual variation in the tropics. *Dynamics of Atmospheres and Oceans*, 44(3–4), 165–183. <https://doi.org/10.1016/j.dynatmoce.2007.05.002>
- Wang, D., Heckathorn, S. A., Mainali, K., & Tripathi, R. (2016). Timing effects of heat-stress on plant ecophysiological characteristics and growth. *Frontiers in Plant Science*, 7, 1–11. <https://doi.org/10.3389/fpls.2016.01629>
- Webb, L., Whiting, J., Watt, A., Hill, T., Wigg, F., Dunn, G., et al. (2010). Managing grapevines through severe heat: A survey of growers after the 2009 summer heatwave in south-eastern Australia. *Journal of Wine Research*, 21(2), 147–165. <https://doi.org/10.1080/09571264.2010.530106>
- Willett, K. M., Dunn, R. J. H., Thorne, P. W., Bell, S., De Podesta, M., Parker, D. E., et al. (2014). HadISDH land surface multi-variable humidity and temperature record for climate monitoring. *Climate of the Past*, 10(6), 1983–2006. <https://doi.org/10.5194/cp-10-1983-2014>
- Xu, Z., FitzGerald, G., Guo, Y., Jalaludin, B., & Tong, S. (2016). Impact of heatwave on mortality under different heatwave definitions: A systematic review and meta-analysis. *Environment International*, 89(90), 193–203. <https://doi.org/10.1016/j.envint.2016.02.007>
- Zhang, S., & Wang, B. (2008). Global summer monsoon rainy seasons. *International Journal of Climatology*, 28, 28–1578. <https://doi.org/10.1002/joc.1659>

References From the Supporting Information

- Buck, A. L. (1981). New equations for computing vapor pressure and enhancement factor. *Journal of Applied Meteorology*, 20(12), 1527–1532. [https://doi.org/10.1175/1520-0450\(1981\)020<1527:NEFCVP>2.0.CO;2](https://doi.org/10.1175/1520-0450(1981)020<1527:NEFCVP>2.0.CO;2)
- Buzan, J. R., Oleson, K., & Huber, M. (2015). Implementation and comparison of a suite of heat stress metrics within the Community Land Model version 4.5. *Geoscientific Model Development*, 8(2), 151–170. <https://doi.org/10.5194/gmd-8-151-2015>

- Coffel, E. D., Horton, R. M., & De Sherbinin, A. (2018). Temperature and humidity based projections of a rapid rise in global heat stress exposure during the 21st century. *Environmental Research Letters*, *13*(1). <https://doi.org/10.1088/1748-9326/aaa00e>
- Coffel, E. D., Horton, R. M., Winter, J. M., & Mankin, J. S. (2019). Nonlinear increases in extreme temperatures paradoxically dampen increases in extreme humid-heat. *Environmental Research Letters*, *14*(8), 084003. <https://doi.org/10.1088/1748-9326/ab28b7>
- Davies-Jones, R. (2008). An efficient and accurate method for computing the wet-bulb temperature along pseudoadiabats. *Monthly Weather Review*, *136*(7), 2764–2785. <https://doi.org/10.1175/2007MWR2224.1>
- Faticchi, S. (2020). *Mann-Kendall test*. Retrieved from <https://www.mathworks.com/matlabcentral/fileexchange/25531-mann-kendall-test>
- Kopp, B. (2020). *WetBulb.m*. Retrieved from <https://github.com/bobkopp/WetBulb.m>
- NOAA. (2021). *Cold & warm episodes by season*. Retrieved from https://origin.cpc.ncep.noaa.gov/products/analysis_monitoring/ensostuff/ONI_v5.php
- Peixoto, J. P., & Oort, A. H. (1996). The climatology of relative humidity in the atmosphere. *Journal of Climate*, *9*(12), 3443–3463. [https://doi.org/10.1175/1520-0442\(1996\)009<3443:TCORHI>2.0.CO;2](https://doi.org/10.1175/1520-0442(1996)009<3443:TCORHI>2.0.CO;2)
- Raymond, C., Matthews, T., & Horton, R. M. (2020). The emergence of heat and humidity too severe for human tolerance. *Science Advances*, *6*(19), eaaw1838. <https://doi.org/10.1126/sciadv.aaw1838>
- Sherwood, S. C., & Huber, M. (2010). An adaptability limit to climate change due to heat stress. *Proceedings of the National Academy of Sciences of the United States of America*, *107*(21), 9552–9555. <https://doi.org/10.1073/pnas.0913352107>
- Stull, R. (2011). Wet-bulb temperature from relative humidity and air temperature. *Journal of Applied Meteorology and Climatology*, *50*(11), 2267–2269. <https://doi.org/10.1175/JAMC-D-11-0143.1>
- Willett, K. M., Dunn, R. J. H., Thorne, P. W., Bell, S., De Podesta, M., Parker, D. E., et al. (2014). HadISDH land surface multi-variable humidity and temperature record for climate monitoring. *Climate of the Past*, *10*(6), 1983–2006. <https://doi.org/10.5194/cp-10-1983-2014>